Supporting Information for

Scattering Evidence of Positional Charge Correlations in Polyelectrolyte Complex Coacervates

Y. Fang, A. M. Rumyantsev, A. E. Neitzel, H. Liang, W. T. Heller, P. F. Nealey, M. V. Tirrell, and J. J. de Pablo

M. V. Tirrell
E-mail: mtirrell@uchicago.edu

J. J. de Pablo
E-mail: depablo@uchicago.edu

This PDF file includes:

Contents

1. RPA Theory of Scattering

A. Inversion of the Structure Factor Matrix in the Salt-Free Case. The elements of the inverse structure factor matrix within the RPA are given by eqs. 6-7 of the manuscript:

$$G_{++}^{-1} = G_{--}^{-1} = \frac{q^2}{6\phi} + \frac{4\pi u f^2}{q^2} + 6w\phi \quad [1]$$

$$G_{+-}^{-1} = G_{-+}^{-1} = -\frac{4\pi u f^2}{q^2} + 6w\phi \quad [2]$$

This matrix can be written as

$$G^{-1} = \begin{pmatrix} \frac{q^2}{A} + \frac{B}{q^2} + C & -\frac{B}{q^2} + C \\ -\frac{B}{q^2} + C & \frac{q^2}{A} + \frac{B}{q^2} + C \end{pmatrix} \quad [3]$$

with $A = 6\phi$, $B = 4\pi u f^2$, and $C = 6w\phi$. It should be inverted. The determinant is given by

$$\det G^{-1} = \left(\frac{q^2}{A} + \frac{2B}{q^2}\right)\left(\frac{q^2}{A} + 2C\right) \quad [4]$$

and the inverse matrix reads

$$G = \frac{1}{\det G^{-1}} \begin{pmatrix} \frac{q^2}{A} + \frac{B}{q^2} + C & \frac{B}{q^2} - C \\ \frac{B}{q^2} - C & \frac{q^2}{A} + \frac{B}{q^2} + C \end{pmatrix} \quad [5]$$

The total structure factor is given by

$$G_{tot}(q) = 2\left(G_{++} + G_{+-}\right) = 2\,\frac{\frac{q^2}{A} + \frac{2B}{q^2}}{\left(\frac{q^2}{A} + \frac{2B}{q^2}\right)\left(\frac{q^2}{A} + 2C\right)} = \frac{C^{-1}}{1 + \frac{q^2}{2AC}} = \frac{(6w\phi)^{-1}}{1 + (q\xi_E)^2} = \sqrt{\frac{3\phi}{\pi u f^2}} \cdot \frac{1}{Q^2 + t} \quad [6]$$

Here the Edwards screening length is defined by $\xi_E^{-2} = 2AC = 72w\phi^2$, $t = r_p^2/\xi_E^2$, and the polymer screening radius of Coulomb interactions is defined by $r_p^{-4} = 2AB = 48\pi u f^2 \phi$. (1) Similarly, polymer charge structure factor reads

$$G_{ch}(q) = 2\left(G_{++} - G_{+-}\right) = 2\,\frac{\frac{q^2}{A} + 2C}{\left(\frac{q^2}{A} + \frac{2B}{q^2}\right)\left(\frac{q^2}{A} + 2C\right)} = \frac{\frac{q^2}{B}}{1 + \frac{q^4}{2AB}} = \frac{1}{Br_p^2} \cdot \frac{(qr_p)^2}{1 + (qr_p)^4} = \sqrt{\frac{3\phi}{\pi u f^2}} \cdot \frac{Q^2}{1 + Q^4} \quad [7]$$

B. Inversion of the Structure Factor Matrix in the Salt-Added Case. The elements of the inverse structure factor matrix within the RPA in the presence of salt are given by

$$G_{++}^{-1} = G_{--}^{-1} = \frac{q^2}{6\phi} + \frac{4\pi u f^2}{q^2 + r_D^{-2}} + 6w\phi \quad [8]$$

$$G_{+-}^{-1} = G_{-+}^{-1} = -\frac{4\pi u f^2}{q^2 + r_D^{-2}} + 6w\phi \quad [9]$$

where $r_D = (4\pi u c_s)^{-1/2}$ is the Debye radius due to small salt ions. This matrix can be written as

$$G^{-1} = \begin{pmatrix} \frac{q^2}{A} + \frac{B}{q^2 + r_D^{-2}} + C & -\frac{B}{q^2 + r_D^{-2}} + C \\ -\frac{B}{q^2 + r_D^{-2}} + C & \frac{q^2}{A} + \frac{B}{q^2 + r_D^{-2}} + C \end{pmatrix} \quad [10]$$

where the definition of the introduced variables remains unchanged, $A = 6\phi$, $B = 4\pi u f^2$, and $C = 6w\phi$. To invert this matrix, we first calculate its determinant:

$$\det G^{-1} = \left(\frac{q^2}{A} + \frac{2B}{q^2 + r_D^{-2}}\right)\left(\frac{q^2}{A} + 2C\right) \quad [11]$$

The inverse matrix equals

$$G = \frac{1}{\det G^{-1}} \begin{pmatrix} \frac{q^2}{A} + \frac{B}{q^2 + r_D^{-2}} + C & \frac{B}{q^2 + r_D^{-2}} - C \\ \frac{B}{q^2 + r_D^{-2}} - C & \frac{q^2}{A} + \frac{B}{q^2 + r_D^{-2}} + C \end{pmatrix} \quad [12]$$

The total structure factor

$$G_{tot}(q) = 2\left(G_{++} + G_{+-}\right) = 2\,\frac{\dfrac{q^2}{A} + \dfrac{2B}{q^2 + r_D^{-2}}}{\left(\dfrac{q^2}{A} + \dfrac{2B}{q^2 + r_D^{-2}}\right)\left(\dfrac{q^2}{A} + 2C\right)} = \frac{C^{-1}}{1 + \dfrac{q^2}{2AC}} = \frac{(6w\phi)^{-1}}{1 + (q\xi_E)^2} = \sqrt{\frac{3\phi}{\pi u f^2}} \cdot \frac{1}{Q^2 + t} \qquad [13]$$

Here the Edwards screening length and the reduced solvent quality t remain unchanged. The charge structure factor changes and, in the presence of salt, is given by

$$G_{ch}(q) = 2\left(G_{++} - G_{+-}\right) = 2\,\frac{\dfrac{q^2}{A} + 2C}{\left(\dfrac{q^2}{A} + \dfrac{2B}{q^2 + r_D^{-2}}\right)\left(\dfrac{q^2}{A} + 2C\right)} = \frac{\sqrt{\dfrac{2A}{B}}}{\dfrac{q^2}{\sqrt{2AB}} + \dfrac{\sqrt{2AB}}{q^2 + r_D^{-2}}} = \sqrt{\frac{3\phi}{\pi u f^2}} \cdot \frac{1}{\dfrac{1}{Q^2 + s} + Q^2} \qquad [14]$$

Here we made use of $\sqrt{2AB} = r_p^{-2}$ and introduced $s = r_p^2/r_D^2$. (1) Finally, the structure factor of polyanions (and polycations, owing to the system symmetry) can be written as

$$G_{++}(q) = G_{--}(q) = \frac{G_{tot}(q) + G_{ch}(q)}{4} = \frac{1}{4}\sqrt{\frac{3\phi}{\pi u f^2}} \cdot \left[\frac{1}{Q^2 + t} + \frac{1}{\dfrac{1}{Q^2 + s} + Q^2}\right] = \frac{1}{4}\sqrt{\frac{3\phi}{\pi u f^2}} \cdot \frac{2Q^4 + Q^2(2s + t) + st + 1}{(Q^2 + t)\left(1 + Q^2 s + Q^4\right)} \qquad [15]$$

We note that a similar RPA-based approach (1, 2) has been earlier used for predicting microphase separation in polyelectrolyte solutions/gels under poor solvent conditions and for interpreting the respective experimental scattering profiles. (3, 4)

C. Total Structure Factor and Osmotic Compressibility. The equilibrium coacervate density is given by the equality of the osmotic pressures, $\Pi = \phi \cdot dF/d\phi - F$, corresponding to the three body repulsive and correlation attractive parts of the free energy. In Θ solvent, $F_{vol} = w\phi^3$ and $\Pi_{vol} = 2w\phi^3$. For the attractive part, one should use

$$F_{corr} = (1 - s)\sqrt{2 + s}\,\frac{\left(48\pi u f^2\right)^{3/4}}{6\sqrt{2}\pi}\phi^{3/4} \qquad [16]$$

and

$$\Pi_{corr} = \frac{\partial F_{corr}}{\partial \phi} + \frac{\partial F_{corr}}{\partial s}\frac{d\phi}{ds} \qquad [17]$$

In the salt-free case, $c_s = 0$ and $s = 0$, the correlation free energy and pressure take simple forms:

$$F_{corr} = \frac{\left(48\pi u f^2\right)^{3/4}}{6\sqrt{2}\pi}\phi^{3/4}; \qquad \Pi_{corr} = -\frac{1}{4} \cdot \frac{\left(48\pi u f^2\right)^{3/4}}{6\sqrt{2}\pi}\phi^{3/4} \qquad [18]$$

The balance between the pressures defines the equilibrium coacervate density

$$\phi_0 = \frac{1}{2^{2/3}\left(3\pi\right)^{1/9}} u^{1/3} f^{2/3} w^{-4/9} \approx 0.49 u^{1/3} f^{2/3} w^{-4/9} \qquad [19]$$

We can now explicitly calculate the Edwards correlation length

$$\xi_E^{-2} = 12\phi_0\left(6w\phi_0 - \frac{3}{16} \cdot \frac{\left(48\pi u f^2\right)^{3/4}}{6\sqrt{2}\pi}\phi_0^{-5/4}\right) =$$

$$12\phi_0\left(2.94 \cdot u^{1/3} f^{2/3} w^{5/9} - 0.74 \cdot u^{1/3} f^{2/3} w^{5/9}\right) = 12\phi_0 \cdot 2.2 u^{1/3} f^{2/3} w^{5/9} \qquad [20]$$

Recall that the osmotic compressibility of the coacervate is given by

$$G_{tot}(q \to 0) = \left[\frac{d\left(\Pi_{vol} + \Pi_{corr}\right)}{d\phi}\right]^{-1} = \left[\phi\frac{d^2\left(F_{vol} + F_{corr}\right)}{d^2\phi}\right]^{-1} \qquad [21]$$

For salt-free Θ solvent, the total structure factor of the system equals

$$G_{tot}(q)|_{c_s=0} = \frac{12\phi_0}{q^2 + \xi_E^{-2}} \to \frac{1}{2.2 u^{1/3} f^{2/3} w^{5/9}} = 0.45 u^{-1/3} f^{-2/3} w^{-5/9} \qquad [22]$$

at $q \to 0$. If the density of the coacervate, ϕ_0, remains unchanged but a lot of salt is added to the system, $F_{corr} \to 0$ and

$$\xi_E^{-2} = 12\phi_0 \cdot (6w\phi_0) = 12\phi_0 \cdot 2.94u^{1/3}f^{2/3}w^{5/9} \quad [23]$$

This results in the structure factor asymptotic behavior

$$G_{tot}(q)|_{c_s\to\infty} = \frac{12\phi_0}{q^2 + \xi_E^{-2}} \to \frac{1}{2.94u^{1/3}f^{2/3}w^{5/9}} = 0.34u^{-1/3}f^{-2/3}w^{-5/9} \quad [24]$$

at $q \to 0$. Thus, the addition of salt should result in the shifting $G_{tot}(q = 0)$ down by approximately 25% as compared to the salt-free case, $0.45/0.34 = 1.32$.

We note that the decrease of $G_{tot}(q = 0)$ is *very sensitive to the solvent quality*. Consider good solvent where two-body repulsions dominate over three-body interactions. For simplicity, assume that excluded volume interactions are described by $F_{vol} = v\phi^2$ while the correlation correction coincides with that obtained for Θ solvent, $F_{corr} = A\phi^{3/4}$. (In fact, in the athermal solvent, $F_{vol} \sim \phi^{9/4}$ (5); for the correlation term, more refined calculations using swollen coil sturture factor (6) suggest that $F_{corr} \sim \phi^{9/11}$). In this case

$$\phi_0 = \left(\frac{A}{4v}\right)^{4/5} \quad [25]$$

$$\frac{d^2F_{vol}}{d\phi^2} = v \quad [26]$$

$$\frac{d^2F_{corr}}{d\phi^2} = -\frac{3}{16}A\phi_0^{-5/4} = -\frac{3v}{4} \quad [27]$$

These estimates show that the osmotic compressibility drop in the athermal is much higher as compared to Θ solvent:

$$\frac{G_{tot}(q=0)|_{c_s=0}}{G_{tot}(q=0)|_{c_s\to\infty}} == \frac{\dfrac{d^2F_{vol}}{d\phi^2}}{\dfrac{d^2F_{vol}}{d\phi^2} + \dfrac{d^2F_{corr}}{d\phi^2}} = \frac{v}{(v - 3v/4)} = 4 \quad [28]$$

This numerical factor equal to 4 better corresponds to the experimentally observed value of 3, suggesting that the solvent quality for the polyelectrolytes is good and that they are locally swollen. This is also consistent with the slope of $-1.6 \approx 1/\nu_+$ in the total structure factor, with $\nu_+ = 0.588$ being the swollen coil exponent.

D. Charge Structure Factor and Correlation Peak in the Athermal Solvent. The RPA analysis in the manuscript's main text was devoted to the case of Θ solvent when PE chains have Gaussian conformations at all length scales. For the athermal solvent, this is not the case because PE chains swell at small length scales, within the concentration blobs. The salt-free coacervate should be viewed as a conglomerate of swollen electrostatic blobs, with self-avoiding random walk statistics inside them. (1, 6–8) At the same time, the PE considered as a chain of the swollen blobs exhibits Gaussian statistics, i.e., polyions retain ideal-coil conformations at the length exceeding the concentration blob size. (8) This is in complete analogy with the neutral semidilute solutions in the athermal solvents. (5) Therefore, the structure factor of PEs has a more complicated form, which does not enable deriving analytics results, which were available for Θ solvent.

However, the approximation for the structure factor can be made to demonstrate the existence of the correlation peak in the athermal solvent (subscript "a"). Screening of Coulomb interactions depends on the PE conformational statistics at the lowest lengths, within the blobs, and is almost independent of that at larger length scales. (1, 8) Therefore, the PE structure factor is approximated by

$$G_{0,a} = \frac{\alpha\phi}{q^{5/3}} \quad [29]$$

where $\alpha \simeq 1$ is a (unknown) numerical constant on the order of unity. Here we have used the Flory value of the critical exponent, $\nu = 5/3$. This structure factor properly describes locally swollen PE statistics. We note that the contributions due to non-Coulomb interactions are absent because the effect of the solvent quality is already taken into account by the appropriate choice of $G_{0,a}(q) \sim q^{-5/3}$. For salt-free coacervates, the inverse elements of the structure factor matrix take the following form:

$$G_{++}^{-1} = G_{--}^{-1} = \frac{q^{5/3}}{\alpha\phi} + \frac{4\pi uf^2}{q^2} \quad [30]$$

$$G_{+-}^{-1} = G_{-+}^{-1} = -\frac{4\pi uf^2}{q^2} \quad [31]$$

In the athermal solvent, the polymer screening radius of Coulomb interactions should be defined as (1, 8)

$$r_{p,a} = \left(8\pi\alpha uf^2\phi\right)^{-3/11} \simeq \left(uf^2\phi\right)^{-3/11} \quad [32]$$

The dimensionless wavevector is hence equal to $Q = qr_{p,a}$. Inversion of the structure factor matrix yields

$$G_{ch,a}(q) = 2\left(G_{++} - G_{+-}\right) = 2\alpha\phi \cdot \frac{q^2}{q^{11/3} + r_{p,a}^{-11/3}} = 2\alpha\phi r_{p,a}^{5/3} \cdot \frac{Q^2}{1 + Q^{11/3}} \quad [33]$$

This functional form of the charge structure factor in the athermal solvent demonstrates that the correlation peak exists. The peak position is given by $Q^* = 1.05$, i.e., $q^* = 1.05 r_{p,a}^{-1} \simeq r_{p,a}^{-1}$. Except for the exact functional form of the structural factor (cf. eqs. 7 and 33) and the other definition of the polymer screening radius, this result for the athermal solvent is in complete analogy with the case of Θ solvent.

In the presence of small salt ions, the inverse structure factor matrix elements are given by

$$G_{++}^{-1} = G_{--}^{-1} = \frac{q^{5/3}}{\alpha\phi} + \frac{4\pi u f^2}{q^2 + r_D^2} \quad [34]$$

$$G_{+-}^{-1} = G_{-+}^{-1} = -\frac{4\pi u f^2}{q^2 + r_D^2} \quad [35]$$

Here the Debye radius is independent of the solvent quality; its definition coincides with that introduced earlier for Θ solvent. By inverting $G_{ij}^{-1}(q)$ matrix one can find the charge structure factor is the presence of salt:

$$G_{ch,a}(q) = 2\left(G_{++} - G_{+-}\right) = 2\alpha\phi \cdot \frac{q^2}{q^{11/3} + \frac{r_{p,a}^{-11/3}}{q^2 + r_D^{-2}}} = 2\alpha\phi r_{p,a}^{5/3} \cdot \frac{1}{Q^{5/3} + \frac{1}{Q^2 + s_a}} \quad [36]$$

Here the reduced salt concentration

$$s_a = \frac{r_{p,a}^2}{r_D^2} = \frac{4\pi u c_s}{\left(8\pi\alpha u f^2 \phi\right)^{6/11}} \sim c_s \phi^{-6/11} \quad [37]$$

remain the linear function of the actual concentration of salt, c_s. It is the value of s_a that governs the position and the very existence of the correlation peak. $s_a \ll 1$ corresponds to the limit of low salt, when the correlation peak exists and its position is given by $Q^* \approx 1$. As salt is added to the system and s_a increases, the peak position shifts to the lower values of Q^*. It completely disappears at $s_a = 0.81$. The limiting case of high salt concentrations corresponds to $s_a \gg 1$. The qualitative evolution of the charge structure factor in the athermal solvent, $G_{ch,a}(q)$, is completely analogous to that in Θ solvent.

It should be finally noted that the inverse structure factors obtained for the athermal solvent within the RPA, $G_{ij}^{-1}(q)$ with $i, j = +, -$, enable correct calculations of the correlation correction to the free energy: (1)

$$F_{RPA} = \frac{1}{2}\int_0^{q_0} \frac{d^3 q}{(2\pi)^3} \ln\left(\frac{\det\left(G_{ij}^{-1}(q)\right)}{\det\left(G_{ij}^{-1}(q)\right)\big|_{u=0}}\right) \quad [38]$$

Unfortunately, for the general salt-added case, $s_a \neq 0$, the integral cannot be calculated analytically. However, for the salt-free case this can be done to obtain $F_{RPA,a} \simeq r_{p,a}^{-3} \simeq \left(uf^2\phi\right)^{9/11}$. (1, 8, 9) By combining this result with the scaling free energy of two-body repulsions in the athermal semidilute solutions, $F_{vol} \simeq \phi^{9/4}$, (5) one can find the equilibrium density of the salt-free athermal coacervate, $\phi \simeq \left(uf^2\right)^{4/7}$. (8) It coincides with the polymer density within the electrostatic blob for the athermal solvent and hence is in agreement with the scaling representation of coacervate in the athermal solvent as a densely packed array of the swollen electrostatic blobs. (7, 8) This agreement demonstrates the validity of the performed RPA analysis for the athermal solvent, particularly the adopted approximation for the PE structure factor, $G_{0,a} \sim q^{-5/3}$, and the idea that screening (and hence correlation attractions) are governed by the local PE statistics within the concentration blob. This supports our theoretical conclusion on the existence and salt-induced decay of the correlation peak in the athermal solvent; it is also consistent with the results of the performed simulations shown in subsection 2C.

2. Simulation Details and Results

A. Simulation Details. Coarse-grained simulations of polyelectrolyte coacervates under Θ solvent conditions are performed using an implicit solvent. Polycations and polyanions are represented by the bead-spring model and both consist of $N = 51$ beads. Non-bonded beads interact with the truncated and shifted Lennard-Jones (LJ) potential

$$U_{LJ}(r) = \begin{cases} 4\varepsilon_{LJ}\Big[\left(\frac{\sigma}{r}\right)^{12} - \left(\frac{\sigma}{r}\right)^{6} \\ \qquad - \left(\frac{\sigma}{r_{cut}}\right)^{12} + \left(\frac{\sigma}{r_{cut}}\right)^{6}\Big], & r < r_{cut} \\ 0, & r \geq r_{cut} \end{cases} \quad [39]$$

Here r is the distance between the beads, σ is the bead size, ε_{LJ} is the LJ interaction parameter, and $r_{cut} = 2.5\sigma$ is the cutoff distance. To simulate Θ solvent conditions, the LJ interaction parameter is set to $\varepsilon_{LJ} = 0.33k_BT$. (11) To simulate good solvent condition, the LJ interaction parameter is set to $\varepsilon_{LJ} = 0.1k_BT$. To simulate athermal solvent condition, the cutoff distance is set to $r_{cut} = 2^{1/6}\sigma$ so the LJ potential becomes purely repulsive, and the LJ interaction parameter is set to $\varepsilon_{LJ} = 1.0k_BT$. The fraction of beads on each polyelectrolyte chain that are charged is $f = 1/3$, with charge valence $z = \pm 1$. Charged beads are evenly distributed along the chain. The Coulomb interactions between charged beads are defined by

$$U_{coul}(r_{ij}) = k_BT\frac{l_B z_i z_j}{r_{ij}} \quad [40]$$

where r_{ij} is the distance between beads with charge valence z_i and z_j. The strength of the Coulomb interaction is characterized by the Bjerrum length, which is set to $l_B = e^2/\epsilon k_BT = 1.0\sigma$, where e is the elementary charge and ϵ is the dielectric constant. The Coulomb potential is evaluated by the particle-particle particle-mesh (PPPM) method (12) with an estimated accuracy of 10^{-4}. Polymer beads are connected into chains through finite-extensible nonlinear elastic (FENE) bonds. The attractive part of the FENE potential is

$$U_{FENE}(r) = \frac{1}{2}k_{spring}R_{max}^2 \ln\left(1 - \frac{r^2}{R_{max}^2}\right) \quad [41]$$

where $k_{spring} = 30k_BT/\sigma^2$ is the spring constant, and $R_{max} = 1.5\sigma$ is the maximum bond length. The repulsive part of the FENE potential is described by a truncated and shifted LJ potential, eq. 39, with $\varepsilon_{LJ} = 1.0k_BT$ and $r_{cut} = 2^{1/6}\sigma$. All beads have the same mass, m. In all simulations, the equations of motion are updated by a velocity-Verlet algorithm with an integration timestep $\Delta t = 0.005\tau_{LJ}$, where $\tau_{LJ} = \sigma(m/k_BT)^{1/2}$ is the standard LJ time. To generate the equilibrium salt-free coacervate, the simulation box is coupled to a Nosé-Hoover barostat with pressure $P = 0$ representing the zero osmotic pressure of polyelectrolytes in the coacervates. A constant temperature is maintained by a Nosé-Hoover thermostat. (13) The equilibrium polyelectrolyte concentration of the salt-free coacervate is $c_p = c_{p,+} + c_{p,-} = 0.388\sigma^{-3}$ in θ solvent, $0.100\sigma^{-3}$ in good solvent, and $0.054\sigma^{-3}$ in athermal solvent. To obtain the coacervate samples for the structure factor calculation, we performed simulations of coacervates with different salt concentrations in the NVT ensemble. For all coacervates considered here, the polyelectrolyte concentrations were kept constant and equal to that of the salt-free one, and charged beads were added to represent salt ions. The salt ion beads, with $z = \pm 1$, interact with each other and polyelectrolyte beads as described by eqs. 39 and 40. The salt concentration, $c_s = c_{s,+} + c_{s,-}$, is varied between 0 and $0.3\sigma^{-3}$ for θ solvent, and between 0 and $0.08\sigma^{-3}$ for good and athermal solvent. The constant temperature is in this case maintained by a Langevin thermostat. All simulations are performed using the software package LAMMPS (13).

B. Monomer Peak in Simulations Scattering Profiles. Figure S1 is identical to Figure 5 of the main manuscript text but shows the structure factors in a wider range of q to demonstrate the monomer peak.

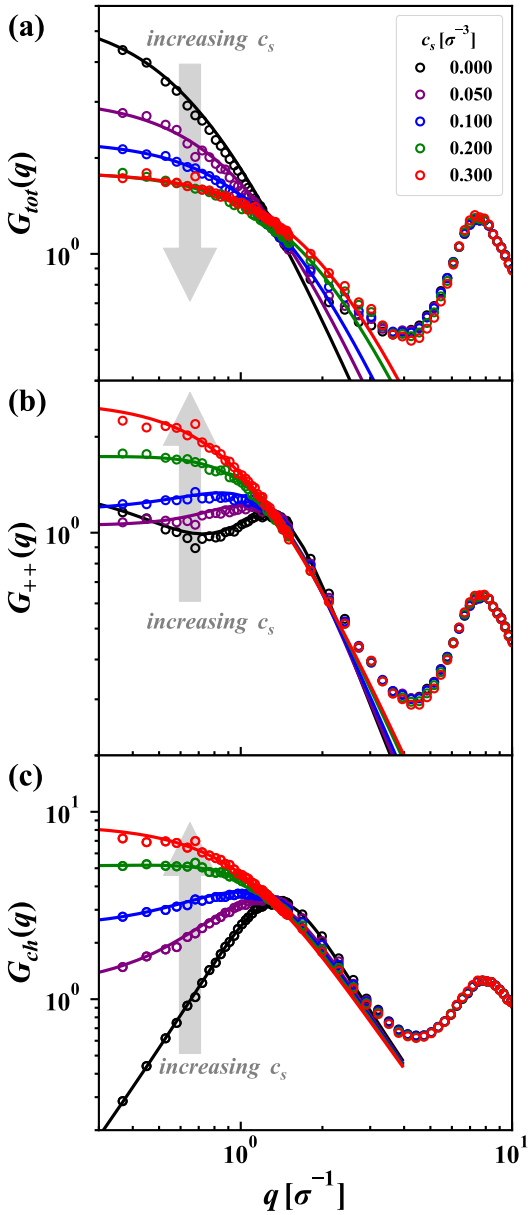

Fig. S1. Structure factor of coacervates under the constant polymer concentration with varying salt concentrations: (a) total structure factor, $G_{tot}(q)$; (b) polycation structure factor, $G_{++}(q)$; (c) charge structure factor, $G_{ch}(q)$; Solid lines are the best theoretical fit, with the functional form given by eqs. 30-32 of the manuscript: $G_{tot}(Q) \propto \left(Q^2 + t\right)^{-1}$, $G_{++}(Q) = (G_{tot}(Q) + G_{ch}(Q))/4$, and $G_{ch}(Q) \propto \left(1/(Q^2 + s) + Q^2 + R\right)^{-1}$.

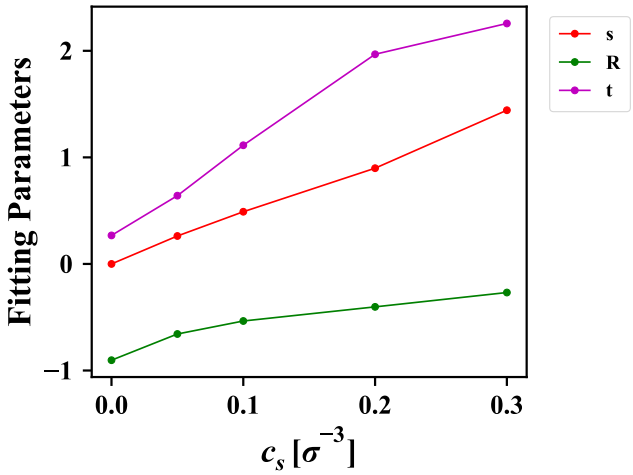

Fig. S2. Dependence of the theoretical parameters s, t, and R, which were used to fit the simulation scattering profiles $G_{tot}(q)$, $G_{++}(q)$, and $G_{ch}(q)$ in Figure 5 of the main text, on the concentration of salt c_s. The reduced salt concentration s increases linearly with c_s, as shown in Figure 6 of the main text. Negative values of R should be attributed to the local packing constraints, which manifest as effective short-range incompatibility between the chains, $\chi_{+-} < 0$. The increase in the parameter t is consistent with the theoretical equation 21 of the main text, which suggests that the Edwards correlation length decreases at increasing c_s. The latter also results in the decreasing osmotic compressibility of the coacervate, $G_{tot}(q \to 0) \propto t^{-1}$, which is observed in simulations and the experiment.

188 **C. Simulation Scattering Profiles for Coacervates in the Athermal and Good Solvent.** The solvent quality controls the $G_{ch}(q)$
189 slope in the range of high q, which reflects the local ideal/swollen coil statistics of the polyelectrolytes.

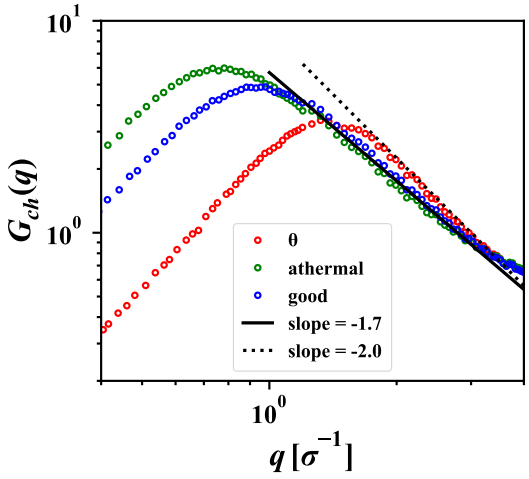

Fig. S3. Charge structure factor of salt-free PECs at different solvent quality from simulations. In θ solvent, the charge structure factor decay with $G_{ch} \sim q^{-2}$ at high q regime, as shown by the dotted black line, indicating the ideal chain conformation in charged blobs. In athermal and good solvent, the charge structure factor decay with $G_{ch} \sim q^{-1.7}$ at high q regime, as shown by the solid black line, indicating the swollen chain conformation in charged blobs.

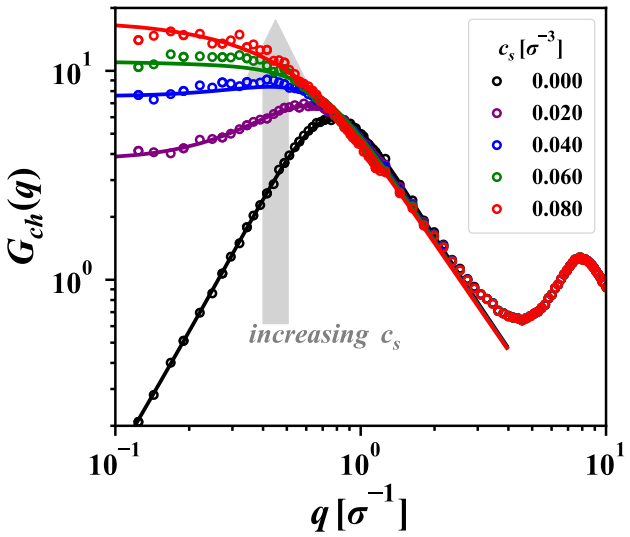

(a) Charge structure factor in athermal solvent

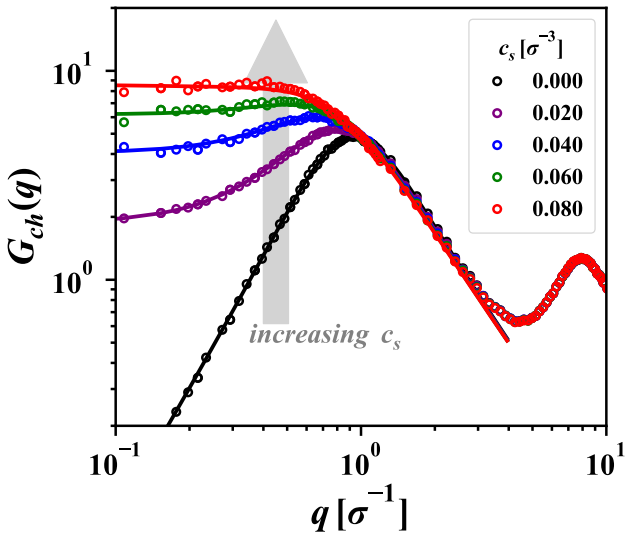

(b) Charge structure factor in good solvent

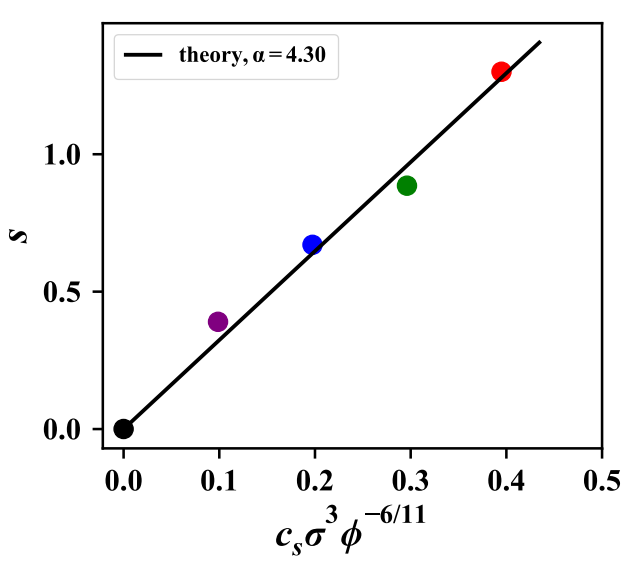

(c) Fitting parameter s in athermal solvent

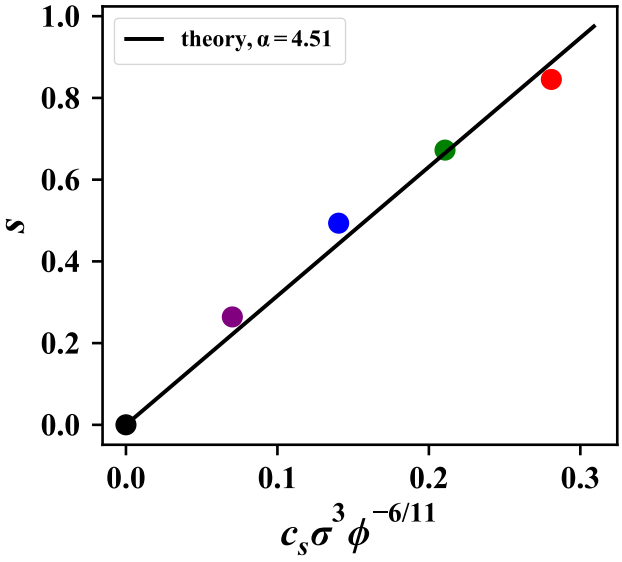

(d) Fitting parameter s in good solvent

Fig. S4. (a-b) Charge structure factor of PECs in (a) an athermal and (b) a good solvent under the constant polymer concentration with varying salt concentrations. Solid lines are the best theoretical fits, with the functional form given by: $G_{ch}(Q) \propto \left(1/(Q^2+s) + Q^{5/3} + R\right)^{-1}$. (c-d) Dependence of the parameter s on salt concentration c_s in (c) athermal and (d) good solvents is linear, in agreement with the RPA predictions, eq. 37. Solid lines are the best theoretical fits of eq. 37 in the Supporting Information, with α being the only fitting parameter.

3. Experimental Details

A. Materials and Methods. All reagents were obtained from Sigma Aldrich and used as received unless otherwise specified. Ethylene oxide (>99%, lecture bottle) was obtained from Praxair, Inc. Poly(AGE_{55}-*stat*-EO_{128}) was synthesized in (10). For the current work this identical neutral precursor was used to generate more copolyelectrolyte material. The deuterated copolyelectrolytes were synthesized as reported previously (10) except that tetrahydrofuran (HPLC grade) from the solvent purification system (MBraun SPS-800) was further purified via vacuum transfer from sodium/benzophenone prior to polymerization. In the current work, all thiol-ene click reactions were conducted in 4/1 dimethylformamide/water as the solvent. Proton nuclear magnetic resonance (^{1}H NMR) spectroscopy was performed using a Bruker Avance III 400 MHz spectrometer collecting 64 scans at a relaxation delay (d1) of 10s. Signals were referenced to the internal standards tetramethylsilane (TMS) in $CDCl_3$ and 3-(trimethylsilyl) propionic-2,2,3,3-d_4 acid, sodium salt in D_2O. ^{1}H NMR spectroscopic data was processed with MestrReNova. Neutral copolymers were characterized by size exclusion chromatography (SEC). Poly(AGE_{55}-*stat*-EO_{128}) was analyzed with 0.01 M sodium bromide in dimethylformamide as the eluent (flow rate = 0.3 mL/min, T = 50 °C) using a Tosoh EcoSEC instrument equipped with three chromatography columns (Tosoh SuperAW3000, SuperAW4000, and guard column) and a refractive index detector. Poly(AGE_{64}-*stat*-d_4-EO_{142}) was analyzed in tetrahydrofuran as the mobile phase (flow rate = 1.0 mL/min, T = 25 °C) using a Shimadzu Prominance LC system equipped with two Agilent PLgel 5 micron Mixed-D columns + a guard column, Wyatt DAWN HELEOS II MALS (658 nm laser) and Wyatt Optilab T-rEX refractive index (RI) detectors.

B. Contrast matching. Contrast matching conditions were calculated (https://www.ncnr.nist.gov/resources/activation/) and measured experimentally for polyelectrolyte solutions (50 mg/mL) using 4 H_2O/D_2O ratios. Results are displayed in Table S1 and Figure S7.

Table S1. Experimentally Measured and theoretically calculated copolyelectrolyte contrast matching conditions and scattering length densities

Chemical	Experimentally measured vol% H_2O / vol% D_2O	Calculated vol% H_2O / vol% D_2O	Experimentally measured SLD [10^{-6}Å^{-2}]	Calculated SLD [10^{-6}Å^{-2}]
H_2O	1		-0.56	
D_2O	0		6.40	
poly($Sulf_{55}$-*stat*-EO_{128})	71.9/28.1	81.3/18.7	1.396	0.741
poly(Am_{ox55}-*stat*-EO_{128})	76.8/23.2	83.3/16.7	1.055	0.599
poly($Sulf_{64}$-*stat*-d_4-EO_{142})	57.9/42.1	55.8/44.2	2.370	2.518
poly(Am_{ox64}-*stat*-d_4-EO_{142})	48.6/51.4	53.6/46.4	3.017	2.671

4. Copolymers and Copolyelectrolytes Characterization Data

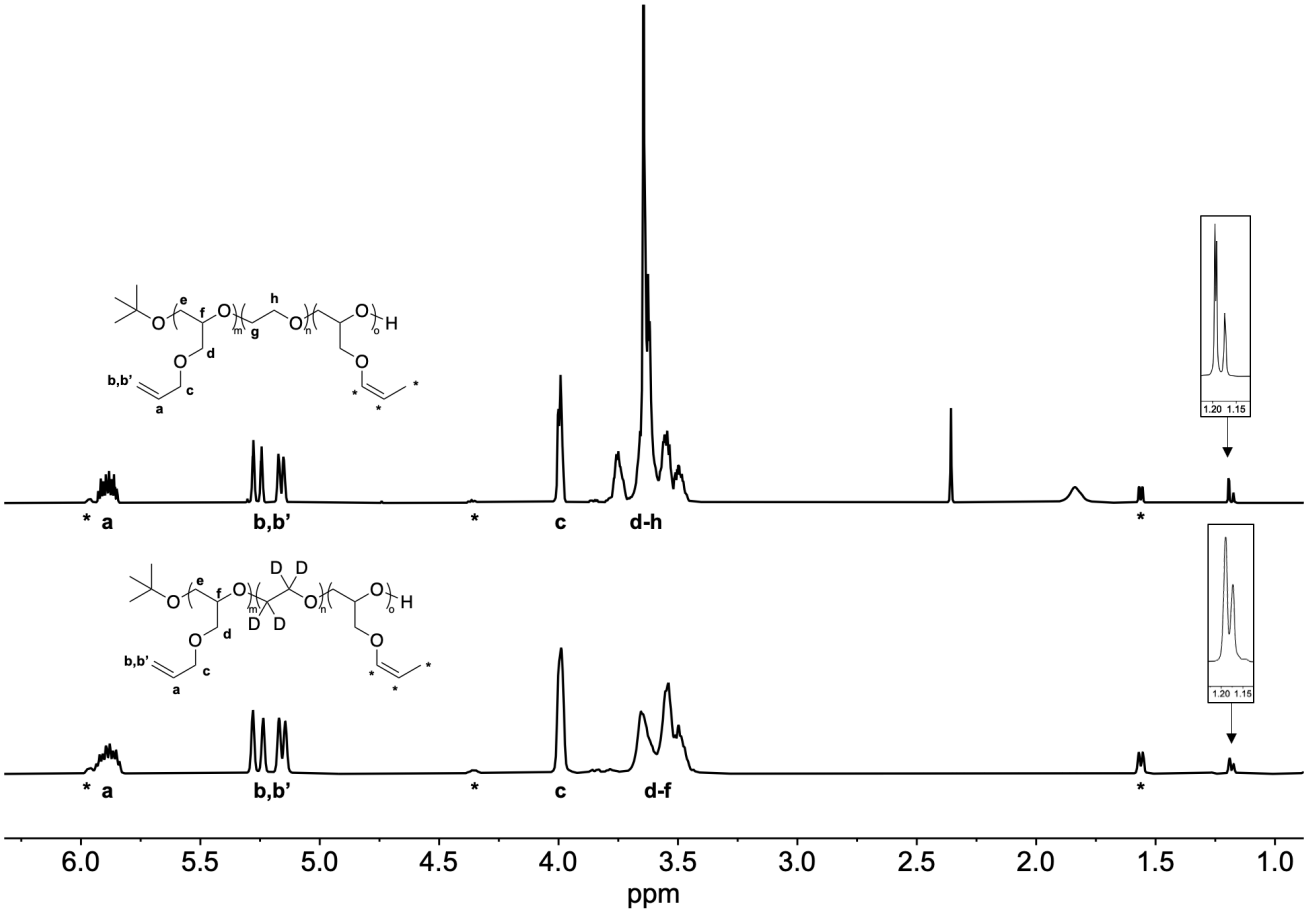

Fig. S5. Overlaid ^{1}H NMR spectra ($CDCl_3$) of Poly(AGE_{55}-*stat*-EO_{128}) and Poly(AGE_{64}-*stat*-d_4-EO_{142}) copolymers synthesized to produce the homologous copolyelectrolytes studied in this work. The end group signal derived from tert-butoxide is magnified and corresponds to 9 protons. Minor signals (*) are attributed to AGE olefins that have isomerized to the internal cis-alkene. The fraction of isomerized alkene units are: Poly(AGE_{55}-*stat*-EO_{128})$\rightarrow$ 6.4% and Poly(AGE_{64}-*stat*-d_4-EO_{142})$\rightarrow$8.7%.

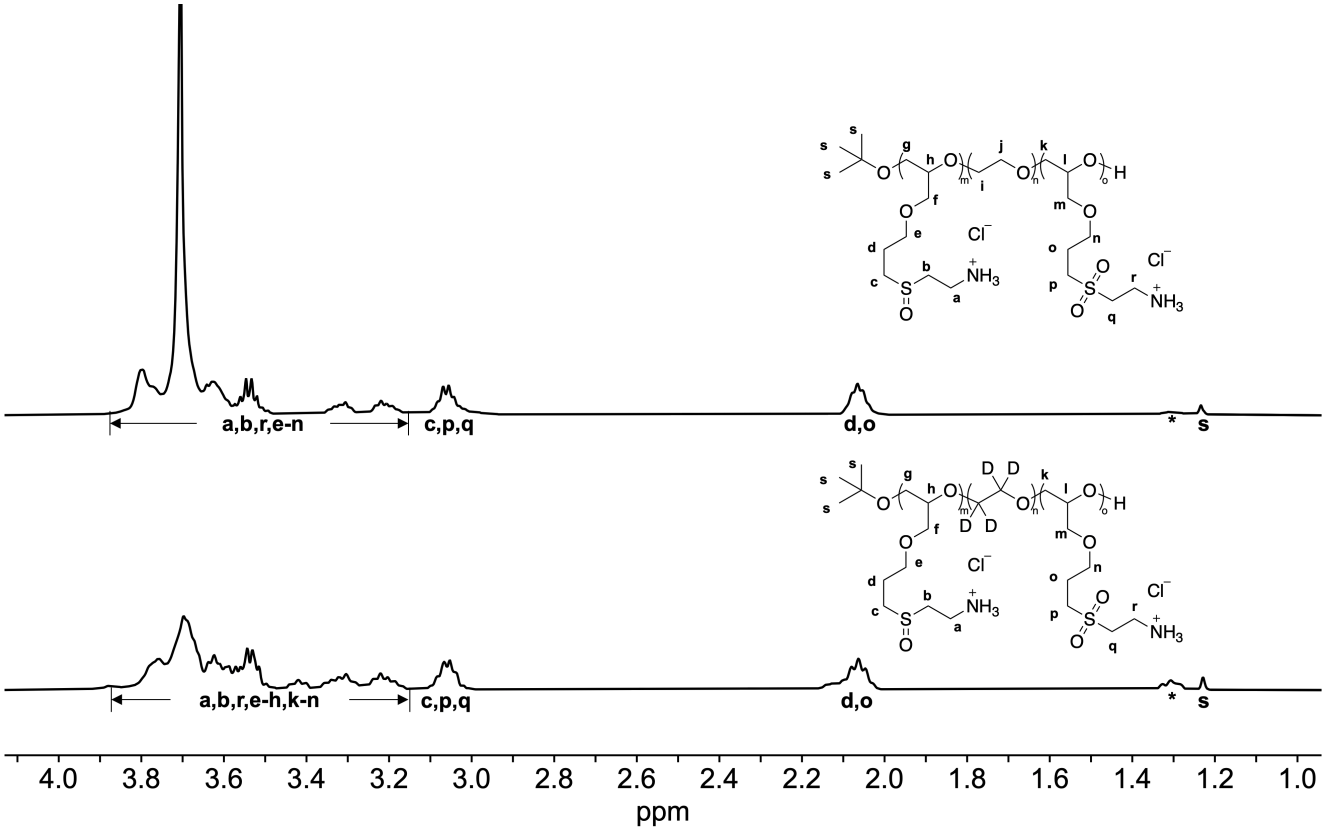

Fig. S6. Overlaid ^{1}H NMR spectra (D_2O) of poly(Am_{ox55}-*stat*-EO_{128}) and poly(Am_{ox64}-*stat*-d_4-EO_{142}) copolycations synthesized from the neutral copolymers in Figure S2 via thiol-ene click functionalization with cysteamine hydrochloride and subsequent oxidation with 2 eq. H_2O_2 relative to moles of sulfur. Minor signals (*) are attributed to products of thiol-ene clicks with isomerized AGE olefins.

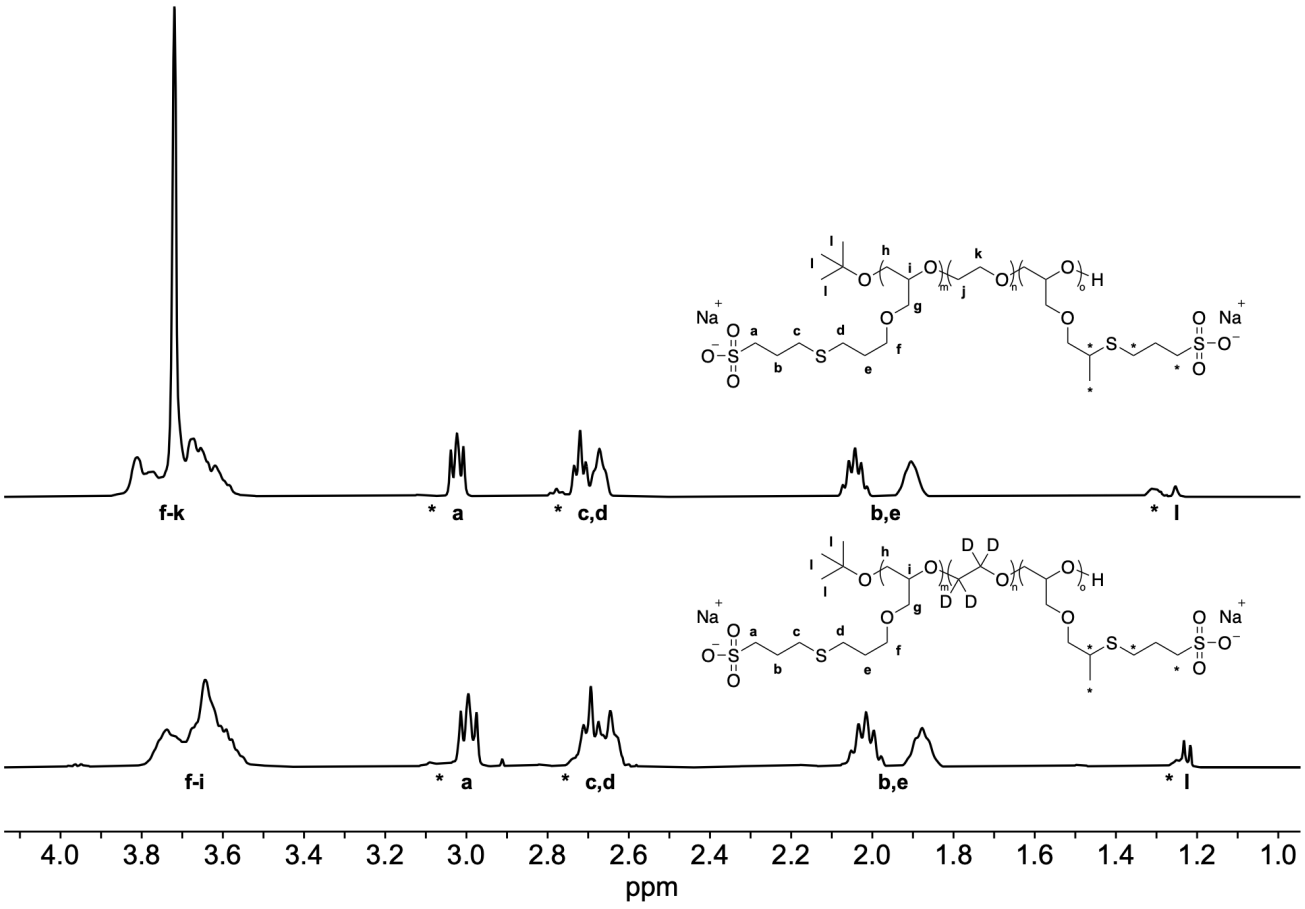

Fig. S7. Overlaid ^{1}H NMR spectra (D_2O) of poly(Sulf$_{55}$-*stat*-EO$_{128}$) and poly(Sulf$_{64}$-*stat*-d_4-EO$_{142}$) copolyanions synthesized from the neutral copolymers in Figure S1 via thiol-ene click functionalization with sodium 3-mercapto-1-propanesulfonate. Minor sigals (*) are attributed to products of thiol-ene clicks with isomerized AGE olefins.

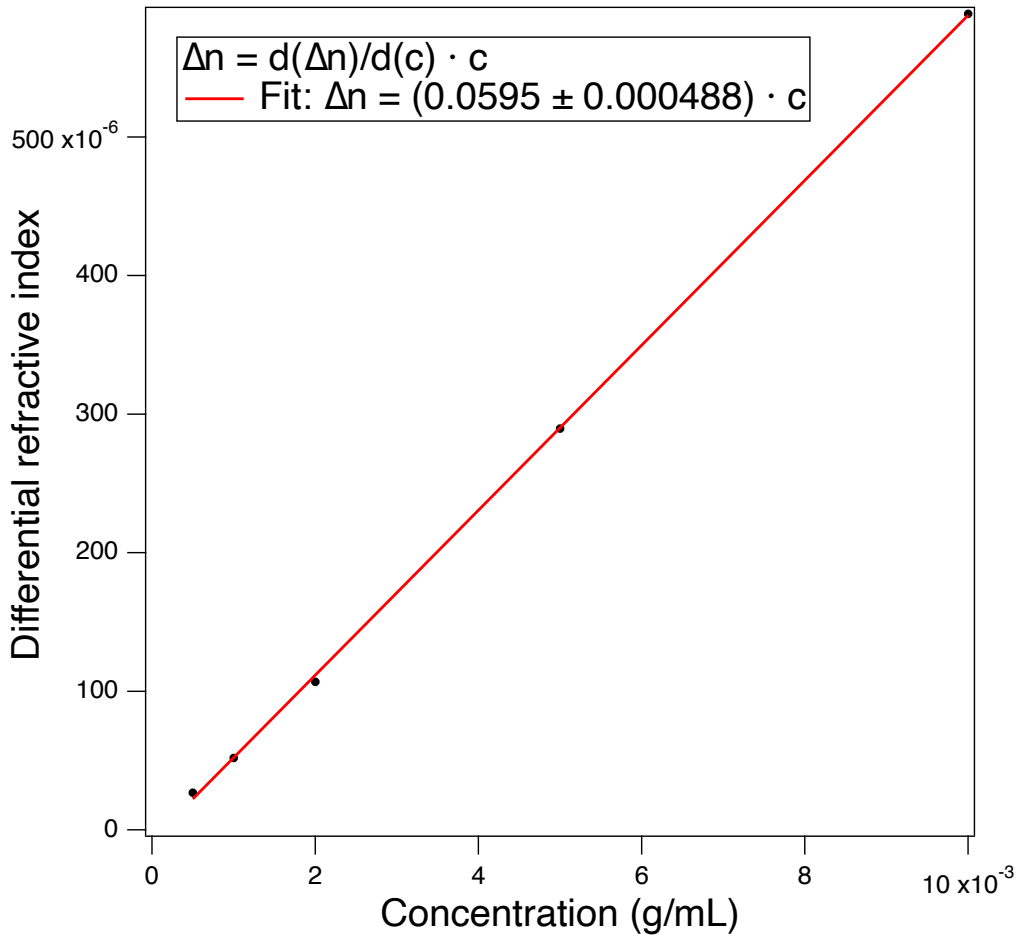

Fig. S8. Batch injections with increasing concentrations of poly(AGE$_{64}$-*stat*-d_4-EO$_{142}$) in THF solution were performed to determine the change in differential refractive index (Δn) as a function of concentration (c). The refractive index increment d(Δn)/dc is calculated from the slope of the graph of differential refractive index (Δn) vs concentration (c).

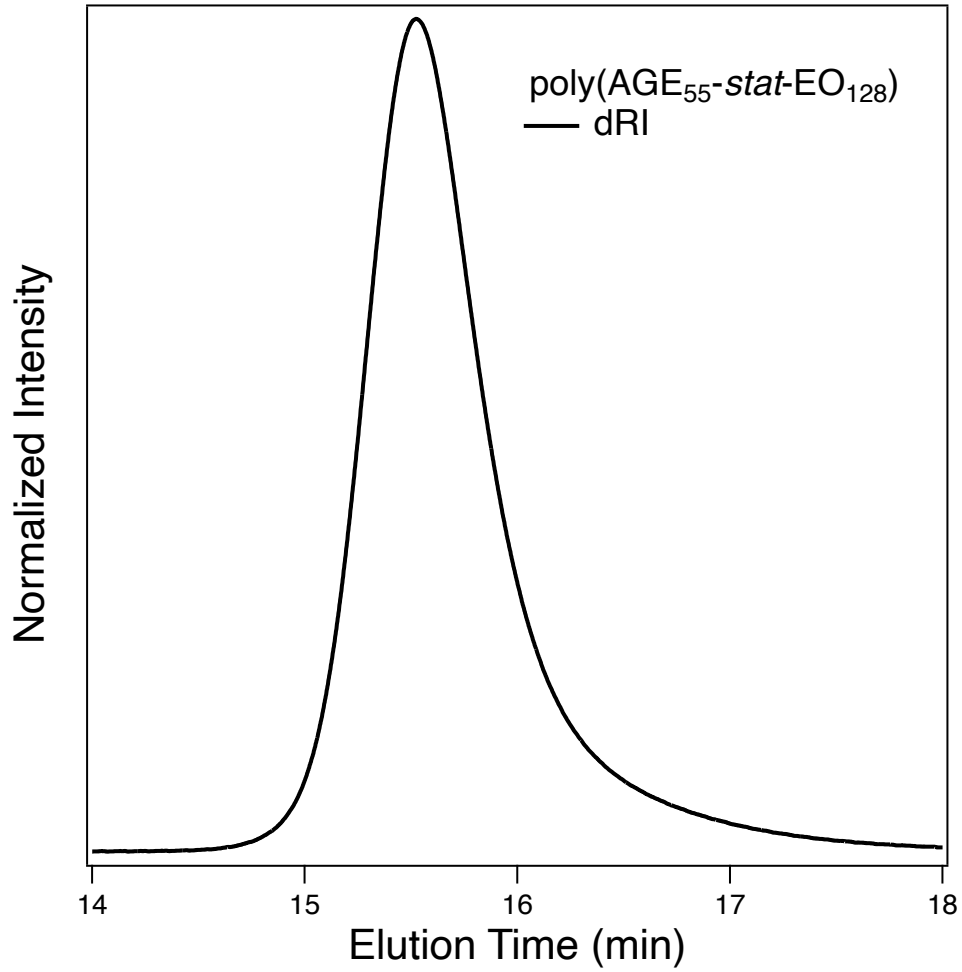

Fig. S9. DMF SEC trace of Poly(AGE_{55}-*stat*-EO_{128}). The sample was prepared in 0.01 M sodium bromide in DMF and eluted at a flow rate of 0.3 mL/min. Dispersity was calculated from the differential refractive index signal which gave $Đ$ = 1.15.

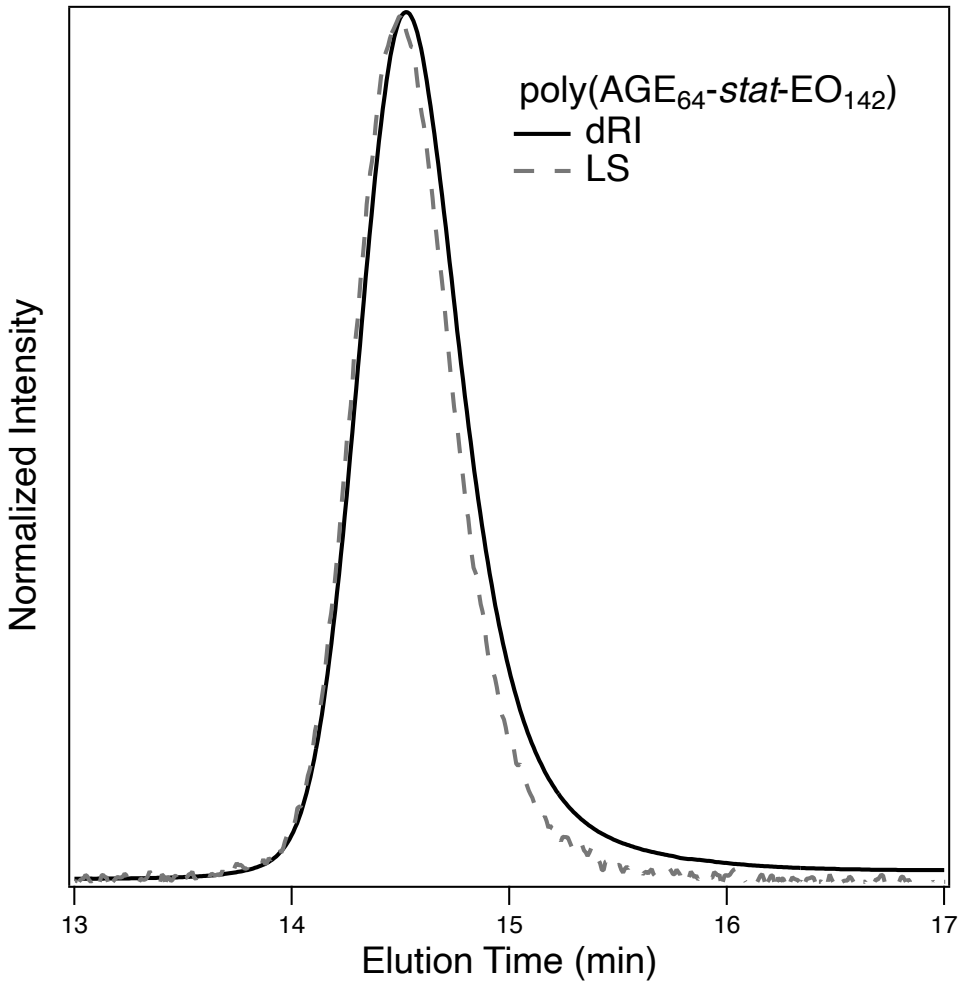

Fig. S10. THF SEC trace of Poly(AGE$_{64}$-*stat*-d_4-EO$_{142}$). The sample was prepared at a concentration of 5mg/mL in THF and eluted at a flow rate of 1.0 mL/min. Molar mass analysis by MALLS provided M_w = 13.77 kg/mol. Dispersity calculated from the light scattering signal gave $Đ$ = 1.05. Dispersity calculated from the differential refractive index signal gave $Đ$ = 1.07.

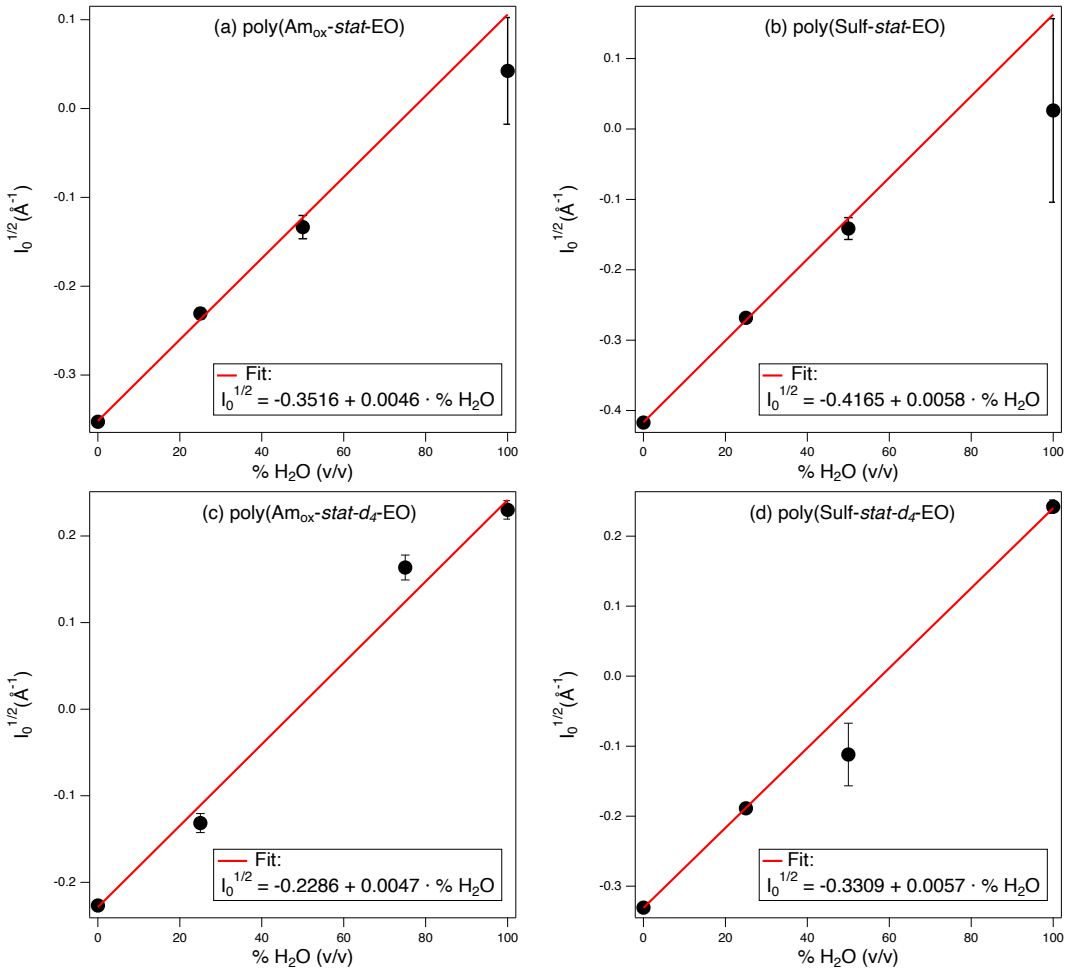

Fig. S11. Contrast matching conditions were determined experimentally by measuring the neutron scattering intensity ($I_0^{1/2}$) for polyelectrolyte solutions (50 mg/mL) with: ϕ_{H_2O} = 0, 0.25, 0.75, and 1. The % H_2O were calculated at $I_0^{1/2}$= 0 to give: (a) poly(Am$_{ox}$-*stat*-EO), % H_2O=76.8; (b) poly(Sulf-*stat*-EO), % H_2O=71.9; (c) poly(Am$_{ox}$-*stat*-d_4-EO), % H_2O=48.6; (d) poly(Sulf-*stat*-d_4-EO), % H_2O=57.9.

References

1. Borue, V. Yu.; Erukhimovich, I. Ya. A statistical theory of weakly charged polyelectrolytes: Fluctuations, equation of state and microphase separation. *Macromolecules* **21**, 3240–3249 (1988).
2. Joanny, J. F.; Leibler, L. Weakly charged polyelectrolytes in a poor solvent. *J. Phys. (Paris)* **51**, 545–557 (1990).
3. Schosseler, F.; Ilmain, F.; Candau, S. J. Structure and properties of partially neutralized poly(acrylic acid) gels. *Macromolecules* **24**, 225–234 (1991).
4. Shibayama, M.; Tanaka, T.; Han, C. C. Small-angle neutron scattering study on weakly charged temperature sensitive polymer gels. *J. Chem. Phys.* **97**, 6842–6854 (1992).
5. P. G. de Gennes, *Scaling Concepts in Polymer Physics* (Cornell University Press, Ithaca, NY, 1979).
6. Borue, V. Yu.; Erukhimovich, I. Ya. A statistical theory of globular polyelectrolyte complexes. *Macromolecules* **23**, 3625–3632 (1990).
7. Z. Wang, M. Rubinstein, Regimes of conformational transitions of a diblock polyampholyte. *Macromolecules* **39**, 5897–5912 (2006).
8. A. M. Rumyantsev, E. B. Zhulina, O. V. Borisov, Complex coacervate of weakly charged polyelectrolytes: Diagram of states. *Macromolecules* **51**, 3788–3801 (2018).
9. J. Qin, J. J. de Pablo, Criticality and connectivity in macromolecular charge complexation. *Macromolecules* **49**, 8789–8800 (2016).
10. A. E. Neitzel, *et. al.*, Polyelectrolyte complex coacervation across a broad range of charge densities. *Macromolecules* **54**, 6878–6890 (2021).
11. G. S. Grest and M. Murat, Structure of grafted polymeric brushes in solvents of varying quality: A molecular dynamics study. *Macromolecules* **26**, 3108–3117 (1993).
12. W. M. Brown, A. Kohlmeyer, S. J. Plimpton, A. N. Tharrington, Implementing molecular dynamics on hybrid high performance computers–particle–particle particle-mesh. *Comput. Phys. Commun.* **183**, 449–459 (2012).
13. S. J. Plimpton, Fast parallel algorithms for short-range molecular dynamics. *J. Comput. Phys.* **117**, 1–19 (1995).